# It is Not About Time - A New Standard for Open-Loop Heliostat Calibration Methods

Max Pargmann[a,1,*], Moritz Leibauer[b,1], Vincent Nettelroth[b], Daniel Maldonado Quinto[a], Robert Pitz-Paal[a]

[a]*German Aerospace Center (DLR), Institute of Solar Research, Linder Höhe, D-51147 Köln, Germany*
[b]*Synhelion Germany GmbH, Am Brainergy Park 1, 52428 Jülich, Germany*

**Abstract**

Heliostat calibration is a vital task in solar tower plants to ensure high plant efficiencies. Currently calibration is performed at close time intervals for every heliostat, to ensure constantly precise heliostat tracking, because it is assumed that a heliostat's precision tends to degrade over time. Consequently, new heliostat calibration procedures are frequently presented that incorporate time-dependent data set splitting for training and testing. In this study, we present a new data-set splitting method that measures the nearest neighbor distance between each calibration point using sun positions in Euler angles (Azimuth, Elevation). We conducted a comparative analysis with the common time-based split method, and our results demonstrate that neither time nor data set size significantly impacted the tracking accuracies. Instead, the distribution of sun position within the data set emerged as the most important factor. Moreover, our findings suggest that using time as a metric can be misleading when reporting validation accuracies. The proposed method has significant implications for the calibration of heliostats, previous and upcoming publications as well as the daily power plant operation. Utilizing this method, the acquired data sets are expected to achieve higher levels of accuracy while requiring less data. Furthermore, it has the potential to enhance the comparability between publications and enable risk-averse assessments of new methods to ensure stated accuracies and improve model evaluation reliability.

*Keywords:* Concentrating solar power, Solar tower power plant, Heliostat aiming, Artificial intelligence, Neural Networks

## 1. Introduction

The efficiency of power plants relies heavily on the ability of heliostats to accurately track the sun. Heliostats must meet strict requirements for accuracy and cost-effectiveness, while also being able to withstand various external factors. There are two main types of heliostat-control: open- and closed-loops.

Closed-loop methods have a higher accuracy, but rely on additional hardware, negatively effecting the cost-effectiveness of the heliostat field.

Open-loop heliostat control is cheaper, but requires direct or indirect measurements and modelling of the heliostat characteristics, making the heliostats' tracking accuracy dependent on the quality of model training. With open-loop control, heliostat calibration is therefore key to maintaining high tracking accuracies. The most commonly used method is the camera-target method (Stone, 1986).

This involves moving a single heliostat from the receiver to a target located close by. Due to individual errors of the heliostat, the intended position of the heliostat may deviate from its measured position. By analyzing this deviation, along with the heliostat's position in the field and the sun's position, an error model can be fitted by regression. This model can then be used to adjust the orientation of the heliostat and minimize its sun tracking error. The method is highly automated and stable, although its accuracy typically falls in the range of 1-5 milliradians. Moreover, AL-Rousan et al. (2020) and Armendariz et al. (2013) found that employing month, day, and time variables to predict tilt and orientation angles performs better than using other variables.

The camera-target method was taken up and improved by a multitude of more advanced approaches, like Heliostat alignment via lasers (Sattler and Göttsche, 2022) and cameras (Burisch et al., 2017) or on the heliostats at night using stars or moonlight (Hines, 2017), measured directly on the receiver (Bern et al., 2020) or drone flights (Gouws, 2018). In general, the number of published calibration methods is vast (Sattler et al., 2020), indicating a significant research effort towards developing and validating analytical procedures for accurate measurements and reliable results. Despite the good published accuracies of these novel approaches, the camera-target method is still the most commonly used method for heliostat calibration in commercial power plants.

This can be explained by the reliability of the stated accuracies. All regression models heavily rely on the collected data set, and power plant operators are taking a big risk

*Corresponding author
*Email address:* max.pargmann@dlr.de (Max Pargmann)
[1]These authors contributed equally to this work.

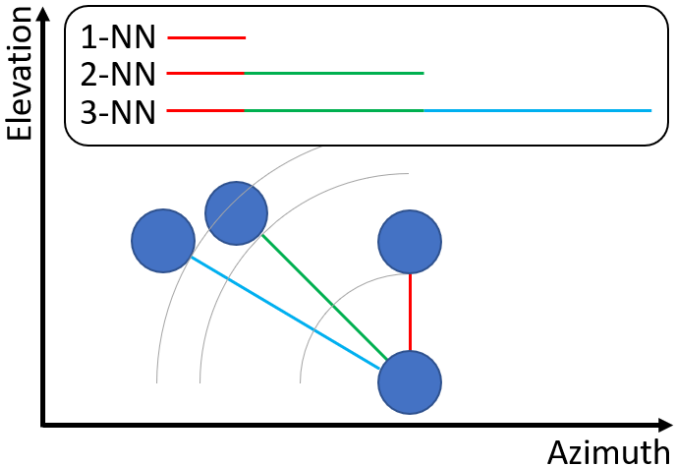


Figure 1: Schematic drawing of the proposed nearest neighbor metric. The shortest distance is measured by the sun position given in Euler coordinates. The heliostat motor positions can be used as well, but do not provide comparability between publications.

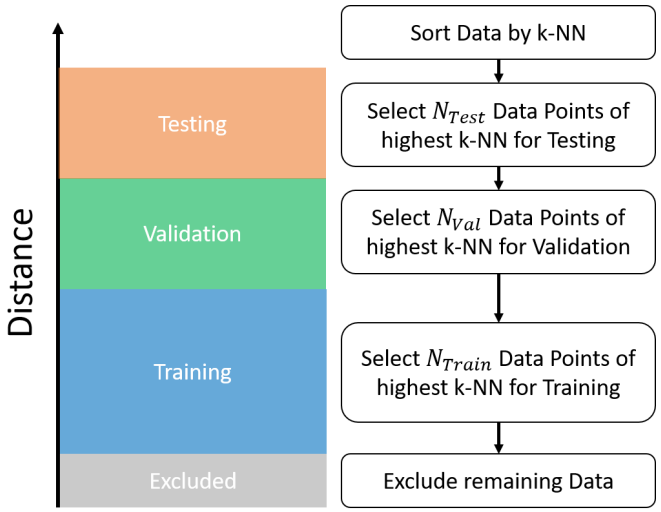


Figure 2: Visual representation of the algorithm to apply the k-NN data set partioning

by exchanging the calibration procedure.

To address this issue, we propose a conservative assumption metric that can be used to risk-averse estimate the yearly heliostat tracking-accuracy and can be quantitatively compared between scientific reports and power plant operators.

The proposed metric evaluates a data set based on the distance between measurements calculated by the sun's Euler angles (Azimuth, Elevation) instead of the time/date of the measurement. By applying this approach to a huge data set from the solar tower in Jülich, we demonstrate that the distribution and balance of the calibration data set with respect to the sun angles have a more significant impact on calibration accuracy than time or data set size. Moreover, we show that data set splits based on time/date can be missleading for reporting heliostat calibration results.

Our proposed metric can further be applied to optimize the data point collection process at solar towers, resulting in higher accuracies with fewer data points. We also give advice for future publication, how to publish results and data sets transparently and comprehensible, accelerating the deployments of new approaches.

## 2. Theoretical Outline

### *2.1. k-Nearest Neighbors Metric*

In machine learning, subsets of all feasible model input combinations are used to extract and learn behavioral patterns and thus accurately predict the effects of before unseen inputs. To cover all such patterns, the training data set should contain samples over the entire range of characteristics. Stochastically, a balanced data set can thus be regarded as a frequency distribution of behavioral patterns over distance to closest recorded data point with low variance. To facilitate the machine learning process, the distribution's mean should furthermore be as low as possible, to cover all patterns adequately. The difficult part for multi-dimensional data points and often unknown pattern distributions is to formulate a balanced distance function over all dimensions.

The heliostat calibration is a regression over the parameter space, sun position, heliostat motor positions and target point to determine and correct the orientation of the heliostat. While the aimpoint is rather static and most often only swaps between operational and calibration target, the solar position changes continuously and thus is the more determining input. The solar position can be quantified either as date and time or as an Euler vector.

Since the solar position directly correlates with the heliostat actuator movements, solar positions relevant to the heliostat's operation can be regarded as indicators for behavioral patterns. In this publication we apply the Nearest Neighbor (NN) distance metric to sort our training, validation and test set (compare Figure 1). The NN is computed as the minimum euclidean distance between a measurement's solar position, represented by azimuth and elevation to another measurement. A data set is optimally balanced if the relevant solar positions' NN distributions' mean and variance are minimal. We also employ k-NN with $k = 1, 2, 3..., k \in \mathbb{N}$. Higher k-NN orders take into account that several measuring points may cluster at one location, but the cluster itself may be separated from the other measurement points. Here, the k-NN behaves like a regional density metric.

We will show, that any sun-distance metric is better suited for evaluating the accuracy of a calibration procedure, than a time dependent split. While this metric is not capable of completely describing the coverage of a point within the data distribution, it is sufficient to be applied as a coverage estimation. Examples for other factors that might affect the coverage, are angles between nearest neighbors,

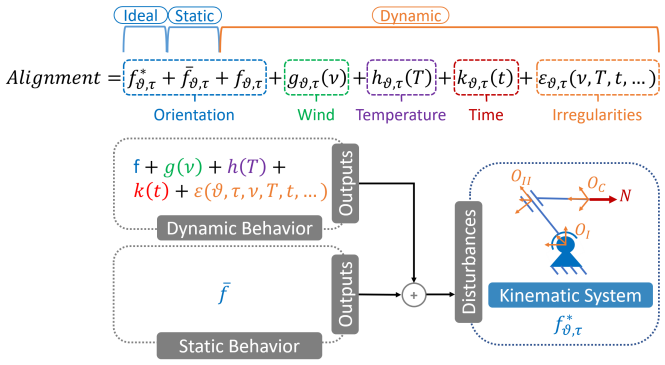


Figure 3: Our kinematic model consists of an ideal heliostat behavior, which can be distorted by up to 28 deficiency parameters (static behavior). Each of these parameters can additionally be modeled by dynamic functions (dynamic behavior).

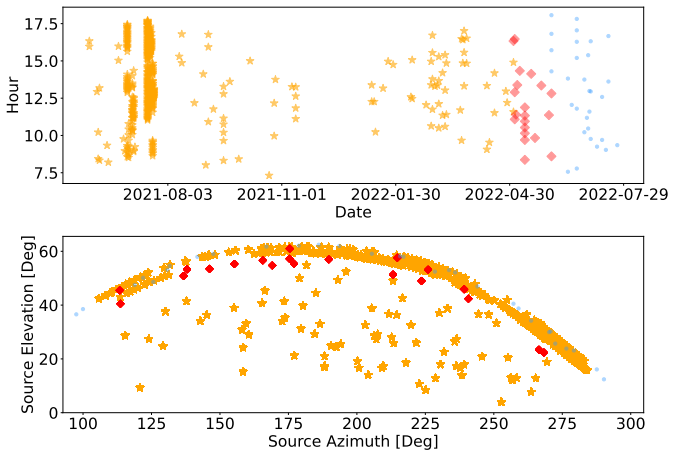


Figure 4: Measurement data from the solar tower in Jülich, gathered by the camera-target method. The upper panel shows the measured data set chronologically using a temporal training-evaluation-test split. The lower panel shows the same split, but plots the measurement data depending on the sun position.

position in the center or at the edges of the distribution and different weightings between azimuth and elevation. Choosing a metric to report calibration accuracies is open to researchers discretion. Nevertheless, the split is crucial and as we will emphasize in the upfollowing chapters, it should be presented transparently.

### 2.2. Data set Splitting

By means of the introduced metric, an ideal testing data set's distance distribution would have a mean and variance of zero to completely cover all behavioral patterns. The same holds true for the evaluation and training data set. Consequently, no ideal distribution can be achieved, if data set splitting is applied. Instead data splitting can be chosen to be as optimal as possible by reducing the data set distributions' mean to cover all behavioral patterns and ensuring data set balancing by reducing the distributions' variance.

A heuristic solution to this optimization problem can be achieved by the algorithm shown in Figure 2. First all data points are sorted by their k-Nearest Neighbor distance to any other available data point. Then, the $N_{test}$ data points of highest distance are selected as testing data points. Thereafter, out of the remaining data points, again the $n_{val}$ data points of highest distance are chosen as validation data. The training data set is constructed from the data that is not selected as testing or validation data. If not all remaining data is selected to construct the training data set, data points of high distance are prioritized.

### 2.3. Comprehensive Heliostat Model

We test our method with a gradient-based regression of well-known machine learning techniques. For this purpose, we have created a comprehensive differentiable heliostat model ( Figure 3). The alignment model's core is a rigid-body kinematic system. This system is modelled in the same way as robotic operating systems (ROS), where each joint forms the origin of a new coordinate system. Each coordinate system can be rotated and translated around all three axes but is part of the coordinate systems chain and thus has six degrees of freedom. Furthermore, manipulating a parent coordinate system affects all its child systems. Using this approach not only allows to compute a heliostat's alignment in global coordinates from its actuator configuration but also to use the coordinate system's inverse principle to gain the actuator configuration from a given target alignment. For this work, heliostats with two or less actuators are regarded, as manipulators of higher degree would require a numerical solver for computing the inverse direction, whereas simpler manipulators' inverse directions can be solved analytically. Therefore, each heliostat has two actuated coordinate systems at each joint plus an additional coordinate system at its concentrator's center point. Taking all degrees of freedom into account, this results in 28 possible parameters for optimization. The model is to our best knowledge universally applicable for all kind of heliostats and deficiency sources. It is written entirely in Pytorch, so the training of the model profits from highly GPU optimized linear algebra. The entire model will be made publicly available[2].

## 3. Measurement Data

For evaluation, we used a calibration data set from the solar tower in Jülich that was collected using the camera-target method. It was chosen for its property of being the largest data set available in the field at the time. All data points were collected during fully automated daily power plant operations, and no additional measurement campaigns were conducted for this publication. However, there are some measurements taken outside of the daily

[2]https://github.com/DLR-SF/holisticDIRC

routine. These measurements were obtained during multiple days of continuous heliostat tracking observations in July 2021. As no further information about this measurement campaign is available, the data must be considered separately. The data set is shown in Figure 4.
In the upper panel, the measurement data is structured chronologically, and a training-test-validation data split is applied, as it would be used at the solar tower and according to literature (ref. Khalsa et al. (2011), AL-Rousan et al. (2020) and Smith and Ho (2014)). A significant number of data points were obtained during the summer months in 2021 due to favorable weather conditions. These measurements appear to be far away from the measurements in the test data set.
In the lower panel, the same data is shown in Azimuth-Elevation representation using the same temporal split as the upper panel. The measurements from summer 2021 cluster here to, but it becomes apparent in this representation that the sun positions of the training and testing data set are very close to each other. Since the data set contains data from over two years we can use it to evaluate the impact of time, sun distribution and data set size separately.

## 4. Proof of Concept at the Solar Tower in Jülich

First we want to verify our assumptions that the sun angle coverage of the data set is a critical parameter for heliostat calibration. To achieve this, we reduced the training data set to a single data point and validated the remaining points based on their NN distance to the training point.
Figure 5 shows the measured data set collected in Jülich. The upper graph shows the data points sorted by their time of measurement. The graph in the middle shows a representation in Euler angles. The color in all plots indicates the time of the measurement and the size of the circles depict the achieved accuracy of the regression.
Both the time-dependent and Euler-angle plots in the upper section indicate a steady increase in error with increasing temporal or spatial distances, which is consistent with AL-Rousan et al. (2020) claim that time is a crucial parameter for calibration. However, some predictions in the time-dependent plots are very accurate despite the huge time distance. Moreover, in the Euler representation very close distant sun positions result in similar predictions, despite the temporal distance. The lower plot supports this observation and contradicts AL-Rousan et al. (2020)'s claim. It suggests that time has only a marginal impact on the results. This plot illustrates the relationship between the distance to the training point and the prediction accuracy. As expected, the accuracy reduces with increasing distance to the training point. However, measurements separated in time do not show any noticeable behavior.
This form of evaluation gets more complicated, when using more than one data point for training and validation, since local distribution effects become of higher importance to the prediction accuracy.

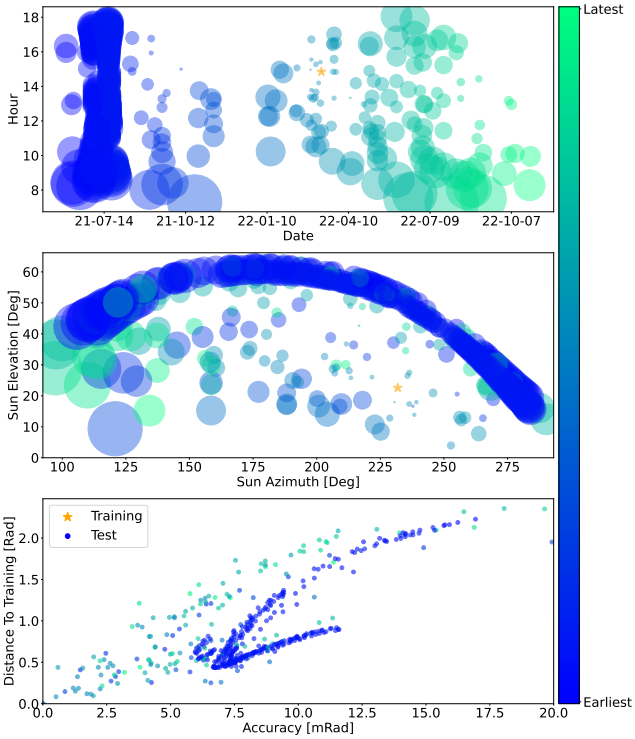


Figure 5: Training with a randomly chosen data point. The upper plot exhibits the validation data arranged chronologically, whereas the middle graph showcases their Euler coordinate representation. Both plots demonstrate an increasing prediction error with greater distances in time or space. The lower plot exhibits a significant correlation between spatial distance and prediction accuracy, characterized by a linear relationship. Conversely, no discernible temporal pattern can be observed in the data.

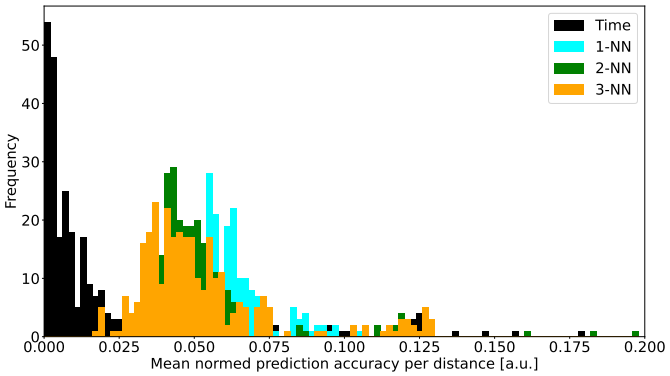


Figure 6: Frequency of achieved accuracies in dependence to the test set distance. For *Time* the distance is measured temporal, for the other sets spatial.

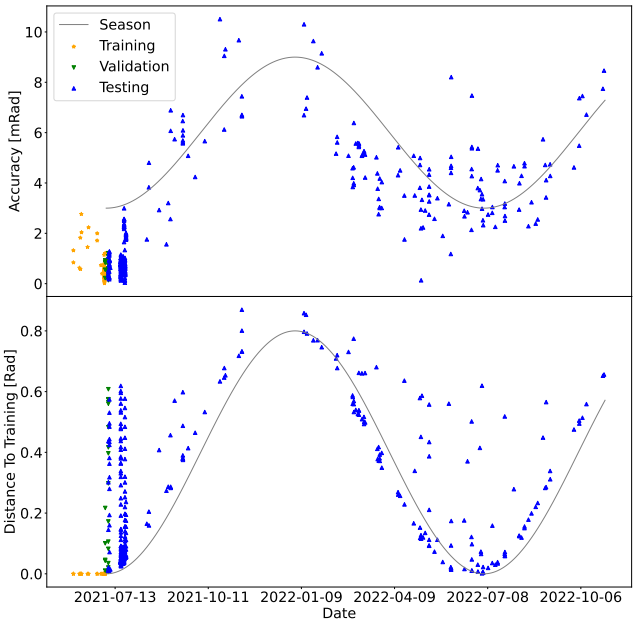


Figure 7: Training with a time-continuous amount of 60 data points for training and 20 for validation. All other data points are then used for testing. A cosine function with a frequency of one year is plotted, referencing seasonal changes.

We will adapt the seasonal sampling approach to verify our thesis by analyzing distinct subsets of the complete data set statistically.

To conduct our seasonal analysis, we used a subset of 110 data points. The first 60 data points, arranged in chronological order, were selected for training the model, followed by the next 30 data points for model validation, and the subsequent 20 data points for testing. After completing the initial round of training and testing, we modified the dataset by removing the oldest day and adding data from the following days until the dataset once again contained 110 data points. By repeating this process, we were able to assess the performance of the heliostat across different seasons, while ensuring that the dataset size remained constant throughout the analysis. The details of this process are described in further detail in the subsequent sections. Then, the model was trained with different training-validation-test partitioning using a time-dependent, and 1-3NN split. We assume, that the accuracy of the prediction is inversely related to the average distance (temporal or spatial) to the training data set. Due to Figure 5 we also expect this behavior to be linear. A non-zero slope indicates the existence of a dependency. In Figure 6 the achieved accuracies of all subsets divided by the mean distance of the subsets validation set to the training set is plotted against their frequency. For the spatial data set splits (1-3NN) this is done by the spatial- and for the time depended split by the temporal-distance. As can be seen, all three spatial data set splits achieve a normal distribution different from zero very close to each other. This indicates a linear slope with some scattering due to measurement uncertainties and local minima in the regression. The time dependent split centers around zero, so we don't see any temporal dependency.

Based on the preceding analysis, it can be inferred that the sun position distribution has a greater impact on the tracking accuracy than time. However, the influence of time cannot be ruled out. In order to further explore the seasonal influence, the first 60 data points were used as training data, the following 20 points as validation data and all other points as testing data. Thus all training and validation data was selected from summer data, while the testing data is distributed over the entire year. The upper plot of Figure 7 illustrates the trained model's prediction accuracies. As expected, validation and training data points are predicted most accurately. The prediction results on the test data set, in contrast are of higher variance. One distinctive feature of the resulting accuracies is a sinusoidal behavior over time with time spans of high and low prediction accuracies. This behavior can be explained by the sun's relative position over the year. For comparison, we added a cosine function plot with frequency of one year and an arbitrary amplitude to Figure 7. The cosine was shifted to match the position of its negative amplitude to the first day within the testing data set. As can be seen, the prediction accuracies' behavior resembles the seasonal curve. Furthermore, prediction accuracies for summer data are generally better than those for data in winter months, due to the fact that training took place in summer. Data points that are separated by a difference of one year show similar results, except for the aforementioned measurement campaign, that performs slightly better. Due to winter months having lower solar elevations and thus greater distances to the training data, the seasonal behavior can also be observed within the data points distances. This is shown in the lower plot of Figure 7.

It should be noted, that independent of the partitioning metric, accuracies between 0.1 and about 10mrad were achieved. Other splits of the data set may result in even

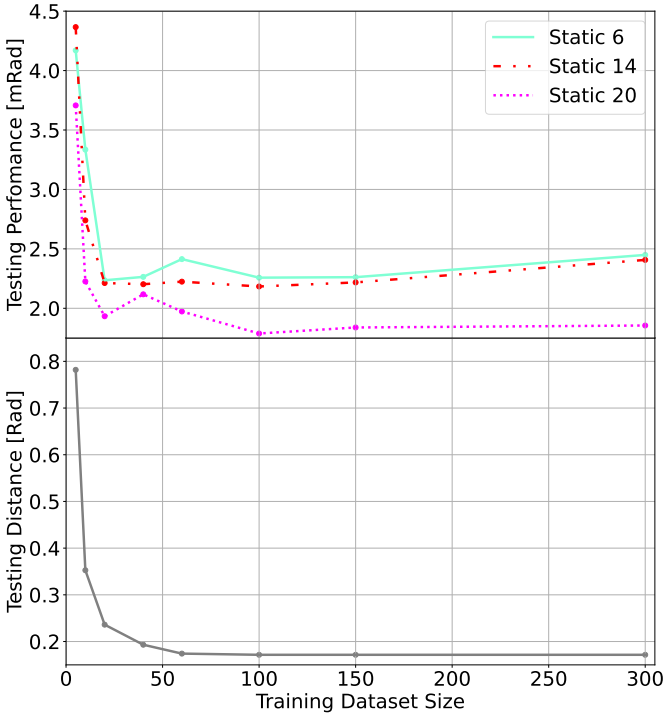


Figure 8: Training accuracies of geometric models using different amounts of free parameters (upper plot). Every stated accuracy is connected with a distance to the evaluation data set (lower plot). This link allows a quantitative comparison between stated accuracies from different data sets.

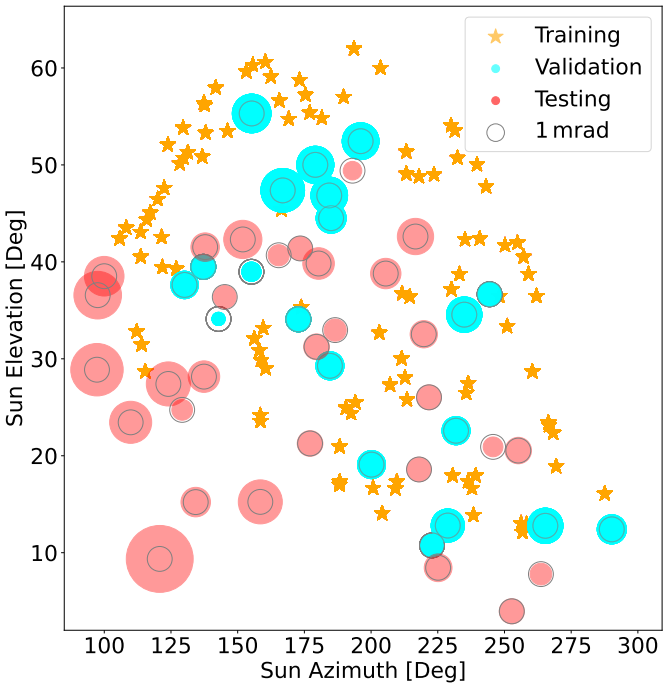


Figure 9: Transparent illustration of the used train-test-validation splits while indicating the prediction error of the test-set error.

higher variances. A published accuracy can therefore only be reasonably evaluated in connection with a corresponding spatial distance to the training data set.

We conducted further analysis to investigate the impact of data set size on heliostat calibration quality, after excluding time as the main parameter. For this, we trained different models on various data set sizes using 3-NN data set splitting. We used a model with 6 parameters (*Static 6*), which utilized the same parameters as those used in Jülich. Additionally, we used a model with 20 free parameters (*Static 20*). The other 8 possible parameters of our model, can lead to unsolvable solutions, so we excluded them from training. And also a model with intermediate number of parameters (*Static 14*).

Figure 8 shows the mean test accuracy plotted against the data set size for all models. The prediction accuracy increases rapidly until 25 data points and then continues to increase until around 100 data points. Beyond that, the accuracy remains relatively constant or decreases slightly. The best accuracy of 1.7 mrad is achieved by the *Static 20* Model at 100 data points.

The plot below also depicts the mean NN distance from the test to the training data set plotted against the data set size. The curve's shape is strongly correlated with the prediction accuracies. When the k-NN value stops decreasing, the accuracy also plateaus. Furthermore, adding more data without reducing the NN distance makes the data set more imbalanced, ultimately reducing accuracy.

From this we can deduce, that the data set size is secondary. A well balanced data set, which reduces the NN-Distance the most, can achieve far better results than a larger unbalanced data set with close packed data points. Finally, and with knowledge from before, we trained our model on 100 training data points using the 3-NN data set split, since it achieved the highest distances to the training data set. The results are shown in Figure 9. The transparent circles indicate a accuracy of 1 mrad, while the colored circles, changing in size indicate the predicted accuracies. It easily becomes apparent, that the data points, inside the region of the training data distribution are very well covered, while the prediction accuracy is strongly reduced at the edges. This is expectable, due to the higher amount of extrapolation. Despite the rather high mean prediction error of 1.7 mrad (compare Figure 8) the plot indicates clearly, that the heliostat behavior will be reliable throughout the year, maintaining or exceeding the reported accuracy, except for operation in early mornings. This can also be reduced by intentionally adding more training data in this regime.

## 5. Implications

### *5.1. On previous publications*

Based on our prior findings, it is apparent that the size of the data set and the time of the measurement period have a subordinate impact on the accuracy of the heliostat calibration. Since this is not covered in literature yet, we will

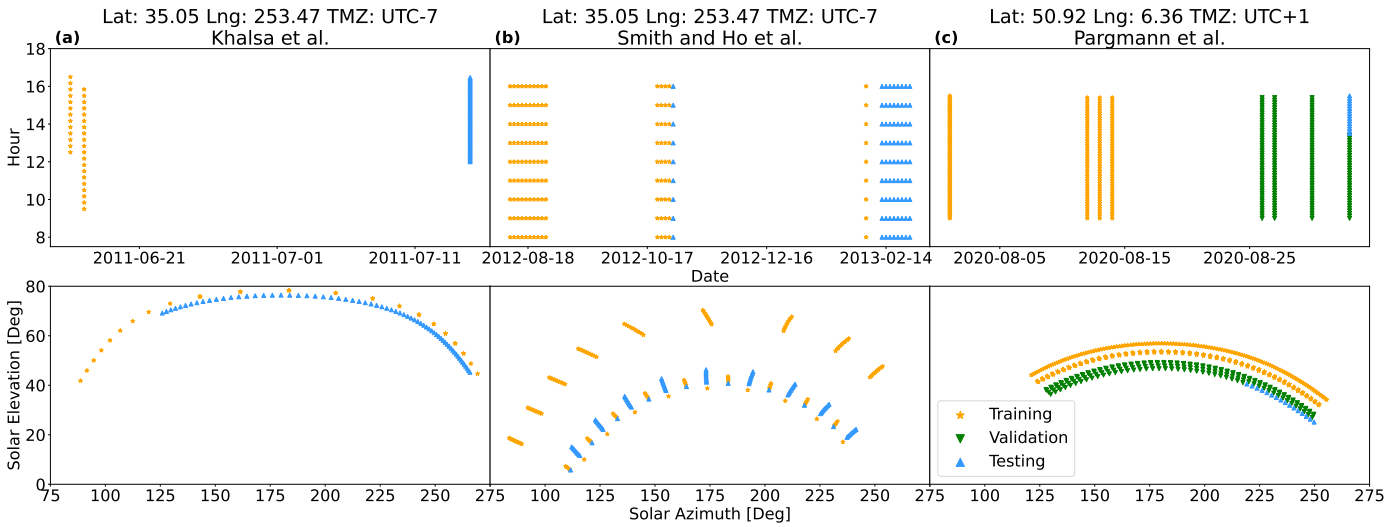


Figure 10: Sun angles selected for training, validation and testing derived from different publications. The upper row represents the temporal representation, the lower the representation in Euler coordinates.

review several publications from recent years about open loop heliostat calibration, which gave enough information about their used data sets to reconstruct their test settings. The sorting corresponds to the date of publication.

1. Khalsa et al. (2011) trained their model on data collected between 12:30pm-4:40pm on June 16 and 9:30am and 3:55pm on June 17, 2011 at an interval of 15-30 minutes and evaluated on data of July 15, 2011 12:53pm to 4:30pm at an interval of 3 to 4 minutes. The authors also stated environmental conditions during their measurements. For plotting, they chose a data representation using hours as the x-axis. A training data set size of (250min + 385min) / (15-30min) was stated, equaling roughly 30 data points. We used the given information to derive a representation in Euler angles (Figure 10 (a) ). Although the training and evaluation set is clearly separated in time, both training and testing data was taken close to the summer solstice and at the same time of day. The mean distance to the training set is below 5°. Since we found a approximately constant behavior in a range of 10°-15° for a standard geometric model, the solar positions might be too similar to assume successfully generalized predictions.
2. Smith and Ho (2014) evaluated their model on a major time difference of six months. Training data was collected between August 9-27 2012, October 22-29 2012 and February 4-5 2013. Two testing campaigns were completed between October 30 to November 1 2012 and February 12-27 2013. Data per heliostat was collected every other day at 1h intervals. The corresponding Euler representation is shown in Figure 10(b) The authors waited a very long time to evaluate their model. However, it is evident that despite a significant time difference between October and February, the solar angles remain similar due to their proximity to the equinox. Due to the one training in February, the mean distance to the training data set is greatly reduced, also affecting the reliability of the method.
3. The study conducted by AL-Rousan et al. (2020) utilized the amount of data as the x-axis. However, due to the absence of time information, an azimuth/elevation representation could not be derived. It can be inferred that the measurements were conducted between December and June, over a period of approximately 15 days. The data set consisted of 153 training samples, and a train/test split ratio of 70:30 was employed. Nonetheless, it was not clear how the separation between the sets was performed, as the different subsets were not labeled in the accompanying plots. Although the authors provided a precise description of their experimental setup, the presentation of their data was insufficiently transparent, which hindered the reproducibility of their findings. Considering the use of degrees (instead of mrad) in the y-axis and the limited information about the data set, further investigation is required to assess the suitability of the reported accuracy for practical applications on solar towers.
4. In a former publication about the heliostat calibration (Pargmann et al. (2021)) we used a similar representation as AL-Rousan et al. (2020). However, the x-axis also states the exact date of measurement. Data was used from the end of July to the mid of August for training, and tested on data starting at the end of August to early February. In Fig. Figure 10(c), the sun positions used for training are determined on the basis of the information given in the paper. With the new presentation, it becomes evi-

dent that the proposed methodology is indeed able to extrapolate to a certain degree. The evaluation and test data is around 10 degrees apart from the training set. However, the test data set is very close to the evaluation and it becomes apparent that the quality of the prediction will drop sharply over the year. This was suspected in the former publication's discussion, but without proof.

No publication is known to us, that used a strict spatial separation (given by sun angles or heliostat axes) of the test or evaluation data set on purpose. In the worst case this means that the evaluation accuracy coincides with the training accuracy and thus a potentially significant overestimation of the achievable accuracy on unknown data.

### *5.2. On upcoming publications*

We highly recommend to present calibration data in upcoming publications using a presentation alike Figure 9 and link stated accuarcies to a corresponding distance to the training set as in Figure 8.
Figure 9 provides valuable insights into the measurement data by demonstrating the performance of the method both within and at the edges of the distribution, as well as facilitating the identification of training, evaluation, and testing data points. This, is crucial, as the data set split greatly affects the resulting accuracy. This representation allows a lot more insights in the used data sets and the stated accuracies than the (commonly proposed) mean error on the entire test data set. The figure establishes reliability and comprehensibility.
Figure 8 serves as a metric for assessing the quality of the prediction by plotting the accuracy against the distance from the training data set. Although the distance might not be the only data set coverage criteria, it is a good quantitative indicator. For example, large training data sets, measured over a single day, can achieve high accuracies in the test set from the same day or in close proximity. However, in such cases, the NN distance may become exceedingly small, reducing the weight of the statement. We highly recommend to present every stated accuracy with a corresponding distance to the training data set. In Figure 8 we additionally presented the impact of data set size. This is not essential, but it is useful for modern approaches utilizing deep neural networks, as the data set separation, coverage and balance becomes increasingly relevant.
The combination of Figure 9 with Figure 8 gives a reliable estimation on how the model performs in intra- and extrapolation. We also recommend utilizing a 3-split strategy for training/evaluation/testing, which is not extensively covered in the literature.

### *5.3. On the Calibration*

The data sets presented in this publication were generated through regular heliostat calibration by means of the camera-target method, with the calibration frequency based on time since the last calibration. The removal of the highest NN-distances from the training data significantly impairs regression results, as valuable information is excluded from training. Therefore, it is not directly applicable for existing data sets from existing power plants. However, this effect can be reduced by gathering the data using the 1-NN-Metric. When a calibration procedure is carried out, the heliostat to be calibrated next is selected by checking which existing data set has the maximum NN-Distance to the current sun position.
Although clustering of measurement points is still possible, it occurs less frequently. Additionally, setting a minimum NN distance further reduces clustering. Due to a better-balanced data set the removal of the most valuable measurement points should be less critical.

Moreover, in Figure 5 we see an approximately constant behavior of the heliostat up to a radial distance of ca. 10° (this may vary between heliostat types). Taking this into account, a data set for each heliostat can be gathered, spanning over all possible sun positions on just 4-5 measurement days, which can be planned in advance. Considering such a data set and our results in this publication, we expect a rather constant heliostat behavior for the next years.

### *5.4. On Daily Power Plant Efficiency Estimation*

Our study shows that the accuracy of heliostats is mainly affected by the position of the sun, rather than time. This crucially affects the prediction accuracy of heliostats for upcoming years. Since the time was mistakenly considered as the primary determinant, the accuracy of a heliostat for the following year could only be estimated coarsely. However, since heliostat accuracy is primarily reliant on the sun positions, precise predictions can be made for any given day of the (next) year, by inserting corresponding sun angles as lines in Figure 9 and interpolating the values of the evaluation data set. The proposed approach yields more accurate predictions than using the mean accuracy.

## 6. Conclusion & Outlook

We were able to clearly show with our results that the coverage of the solar positions is the most relevant quantity for the heliostat calibration and not the time or data set size, as often assumed. Furthermore, we could show that time can be missleading with respect to the training/evaluation data split. It can happen unintentionally that, despite a large temporal distance, similar sun positions are used and thus local overfitting instead of generalization can occur. The method, we propose, can be used two ways. First to improve the prediction quality of existing models in the long term and to reduce the data set required for this purpose. Second, it should also serve as a blueprint for future publications. The representation of the measured points in Euler coordinates is important for the interpretation of

stated accuracies. We believe that a presentation of the measurement data and results as shown in this publication offers reliability and thus better acceptance for power plant operators as well as scientifically providing for more transparency and comprehensibility in this area.

## References


K. W. Stone, Automatic heliostat track alignment method, 1986. US Patent 4,564,275.

N. AL-Rousan, N. A. M. Isa, M. K. M. Desa, Efficient single and dual axis solar tracking system controllers based on adaptive neural fuzzy inference system, Journal of King Saud University-Engineering Sciences 32 (2020) 459–469.

J. Armendariz, C. Ortega-Estrada, F. Mar-Luna, E. Cesaretti, Dual-axis solar tracking controller based on fuzzy-rules emulated networks and astronomical yearbook records, in: Proceedings of the world congress on engineering, volume 1, 2013, pp. 3–5.

J. C. Sattler, J. Göttsche, Progress in the development of a laser and camera system for the calibration of heliostat fields of central receiver systems, in: AIP Conference Proceedings, volume 2445, AIP Publishing LLC, 2022, p. 070011.

M. Burisch, L. Gomez, D. Olasolo, C. Villasante, Heliostat kinematic system calibration using uncalibrated cameras, in: AIP Conference Proceedings, volume 1850, AIP Publishing LLC, 2017, p. 030007.

Hines, Heliostat characterization using starlight, 2017. US Patent US20180299264A1.

G. Bern, M. Bitterling, P. Schöttl, A. Ferriere, Y. Volut, A. Heimsath, P. Nitz, Experimental assessment of simultaneous in-situ heliostats calibration methodology heliocontrol at themis facility, in: AIP Conference Proceedings, volume 2303, AIP Publishing LLC, 2020, p. 030005.

J. E. Gouws, Calibration of heliostats using a drone., Ph.D. thesis, Stellenbosch: Stellenbosch University, 2018.

J. C. Sattler, M. Röger, P. Schwarzbözl, R. Buck, A. Macke, C. Raeder, J. Göttsche, Review of heliostat calibration and tracking control methods, Solar Energy 207 (2020) 110–132.

S. Khalsa, C. Ho, C. Andraka, An automated method to correct heliostat tracking errors, Proceedings of SolarPACES (2011) 20–23.

E. Smith, C. Ho, Field demonstration of an automated heliostat tracking correction method, Energy Procedia 49 (2014) 2201–2210.

M. Pargmann, D. Maldonado Quinto, P. Schwarzbözl, R. Pitz-Paal, High accuracy data-driven heliostat calibration and state prediction with pretrained deep neural networks, Solar Energy 218 (2021) 48–56. URL: https://www.sciencedirect.com/science/article/pii/S0038092X21000621. doi:https://doi.org/10.1016/j.solener.2021.01.046.